ACS OMEGA

http://pubs.acs.org/journal/acsodf

Article

Targeted Isolation of Dolabellane Diterpenoids from the Soft Coral *Clavularia viridis* Using Molecular Networking

Xin Dong,[§] Jingshuai Wu,[§] Hongli Jia, Shan Cen, Wei Cheng,* and Wenhan Lin*

Cite This: *ACS Omega* 2023, 8, 21254−21264

Read Online

ACCESS | Metrics & More | Article Recommendations | Supporting Information

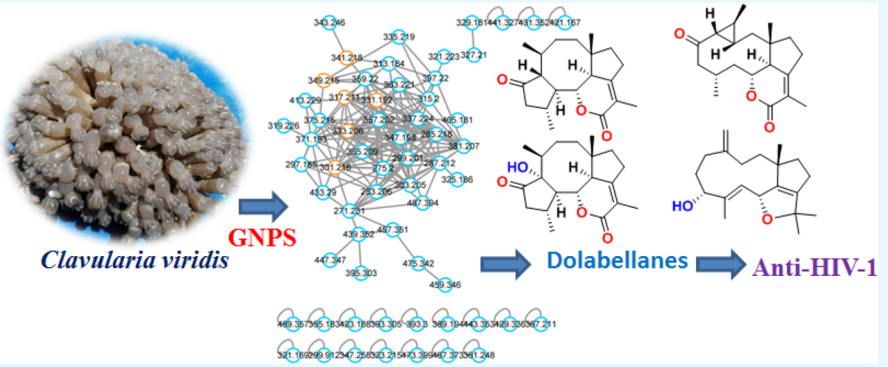

ABSTRACT: LC−MS/MS-based molecular networking annotation coupled ^{1}H NMR detection allowed the depiction of the soft coral *Clavularia viridis* to produce a profile of dolabellane-type diterpenoids. Chromatographic separation of the EtOAc fraction resulted in the isolation of 12 undescribed dolabellane-type diterpenoids, namely, clavirolides J−U (**1**−**12**). Their structures were characterized by the extensive analysis of the spectroscopic data, including the calculated ECD and X-ray diffraction for the configurational assignments. Clavirolides J−K are characterized by a 1,11- and 5,9-fused tricyclic tetradecane scaffold fused with a *α*,*β*-unsaturated-*δ*-lactone, and clavirolide L possesses a 1,11- and 3,5-fused tricyclic tetradecane scaffold, which extend the dolabellane-type scaffolds. Clavirolides L and G showed significant inhibition against HIV-1 without RT enzyme inhibition, providing additional non-nucleosides with different mechanisms from efavirenz.

INTRODUCTION

Dolabellane-type diterpenoids are structurally characterized by the presence of a unique [9.3.0] cyclotetradecane skeleton,[1−3] which is distinct from other natural cyclotetradecane skeletons such as cembranes, briaranes and eunicellanes.[4,5] These metabolites are widely distributed in marine and terrestrial organisms, of which marine-derived corals (soft corals and gorgonians) predominate the production of dolabellane-related analogues.[6] The structural variation of the analogues from different origins is mainly attributed to the olefinic rearrangement and oxidation at the backbone, with the exception of soft-coral-derived clavirolides and clavularinlides that are fused by an unsaturated *δ*-lactone to extend the scaffold diversity.[7,8] These findings imply that marine benthic corals confront more competitive environments than other organisms, thus generating structurally diverse metabolites for chemical defense. Dolabellanes exhibit cytotoxic, antibacterial, antifungal, antiviral, antimalarial, molluscicidal, ichthyotoxic, and phytotoxic activities,[9] of which dolabelladienetriol is a potent inhibitor of the HIV-1 replication in primary cells *in vitro* through the inhibition of the enzyme RT.[10] These findings have attracted our attention to explore marine soft corals for the discovery of structurally novel diterpenes with potent bioactivities.

LC−MS/MS-based molecular networking provides an effective tool to distinguish the structure features from a metabolic profile. Among the developed strategies, the Global Natural Product Social Molecular Networking (GNPS) platform is widely used for the dereplication and recognition of target metabolites.[11−13] In the present work, LC−MS/MS-based molecular networking coupled to molecular annotation by the molecular networking workflow on the GNPS platform[14,15] was used to screen the coral species from the in-house coral library, and the soft coral *Clavularia viridis* was selected for further chemical examination because of the metabolite cluster annotated to dolabellane-related diterpenes (Figure 1), of which clavirolides F (*m*/*z* 333 [M + H]$^+$),[16] B, D, E, I (*m*/*z* 317 [M + H]$^+$),[17,18] C (*m*/*z* 341 [M + Na]$^+$),[17] and G (*m*/*z* 301 [M + H]$^+$);[7] clavularinlides A (*m*/*z* 331 [M +

Received: April 12, 2023
Accepted: May 15, 2023
Published: May 26, 2023

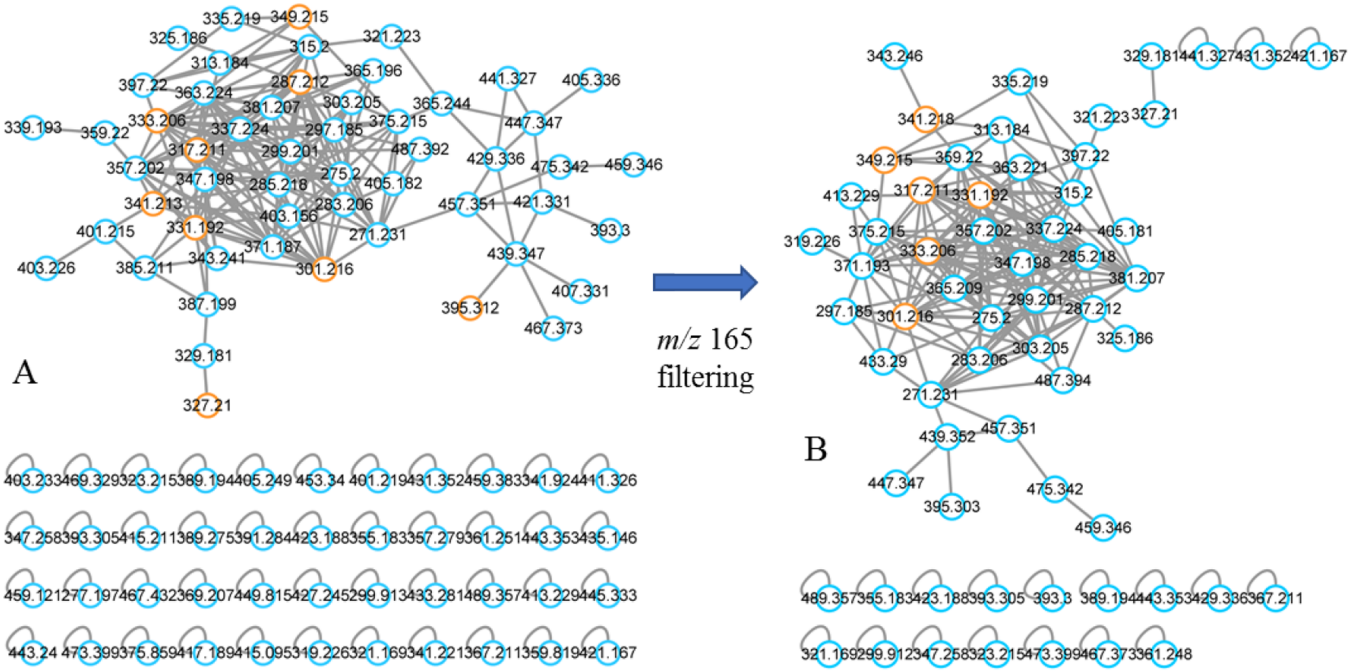

Figure 1. LC−MS/MS molecular networking of the EtOAc extract of *C. viridis*. (A) Molecular networking with the clusters correlating to dolabellane-type diterpenoids. (B) Daughter ion at *m/z* 165 filtering criterion for a subcluster of the molecular network. Orange spots: annotated dolabellanes.

H]$^+$) and B (*m/z* 349 [M + H]$^+$);[8] clavufuranolide C (*m/z* 287 [M + H]$^+$);[19] and clavinflols C (*m/z* 395 [M + Na]$^+$)[20] and A (*m/z* 327 [M + Na]$^+$)[21] were characterized. These dolabellane analogues were subsequently obtained by chromatographic separation, and their structures were identified by the spectroscopic data in comparison with those reported in the literature. However, many unidentified nodes within the molecular cluster imply a number of undescribed dolabellanes waiting for chemical examination. Analysis of the fragment features of clavirolide G and relevant analogues bearing an unsaturated δ-lactone in the molecular cluster by the mzCloud-Advanced Mass Spectral Database revealed these molecules sharing a common daughter ion at *m/z* 165. Using this ion as a filtering criterion, a subcluster of the molecular network structurally related to clavirolide G was generated (Figure 1B). Targeted isolation from the correlated peaks in the LC spectrum by chromatographic methods led to the isolation of clavirolides J−U (**1**−**12**).

RESULTS AND DISCUSSION

Clavirolide J (**1**) was obtained as a colorless crystal, and its molecular formula was assigned to $C_{20}H_{28}O_3$ based on the HRESIMS data, requiring seven degrees of unsaturation. The IR absorptions at 1709 and 1736 cm^{-1} suggested the presence of ketone and lactone functionalities. The ^{13}C NMR (APT) data indicated the presence of 20 carbon resonances, including two olefinic carbons for a double bond and two carbonyl groups (Table 2). These data suggested a tetracyclic diterpene framework. In addition, the HSQC data directly correlated the protons to the corresponding carbons, of which four methyls, five methylenes, and six methines were classified. The COSY correlations afforded a spin system of H_2-2 (δ_H 1.68, 1.70)/H_2-3 (δ_H 1.55, 1.93)/H-4 (δ_H 1.74)/H-5 (δ_H 1.73)/H-9 (δ_H 2.02, ddd, *J* = 6.2, 8.0, 10.0 Hz)/H-8 (δ_H 2.23, m)/H_2-7 (δ_H 2.09, 2.39), and the extended correlations of H-4 to H_3-16 (δ_H 1.06, d, *J* = 6.2 Hz) and H-8 to H_3-17 (δ_H 1.42, d, *J* = 7.0 Hz) were assignable for the location of methyl groups at C-4 (δ_C 37.1) and C-8 (δ_C 33.3). In addition, COSY relationships from H-10 (δ_H 4.02, dd, *J* = 10.0, 11.4 Hz) to H-9 and H-11 (δ_H 2.70, d, *J* = 11.4 Hz) were observed. In association with the HMBC correlations from H-5 (δ_H 1.73, m) and H_2-7 to a ketone carbon C-6 (δ_C 217.5), a cyclopentanone unit (ring A) was assigned. The HMBC correlations from H_3-15 (δ_H 0.98, s) to C-1 (δ_C 44.2), C-2 (δ_C 34.0), and C-11 (δ_C 52.6) along with the mentioned spin systems allowed the fusion of a cyclooctane ring (ring B) to ring A across C-5 (δ_C 54.0) and C-9 (δ_C 54.4). A cyclopentane ring as the third ring (ring C) connected to C-1 and C-11 of ring B was confirmed on the basis of the COSY relationship between H_2-13 and H_2-14 in addition to the HMBC correlations of H_3-15 to C-14 (δ_C 44.1) and H_2-13 to C-11 and C-12 (δ_C 161.6). Moreover, the fusion of an unsaturated δ-lactone across rings B and C at C-10 (δ_C 83.8) and C-12 was evident from the HMBC correlations of H_3-19 (δ_H 1.84, s) to C-12, C-18 (δ_C 120.3), and C-20 (δ_C 165.6) and between H-10 and C-20. Therefore, a 5,8,5-tricyclic scaffold fused by an unsaturated δ-lactone ring was established.

https://doi.org/10.1021/acsomega.3c02429
ACS Omega 2023, 8, 21254−21264

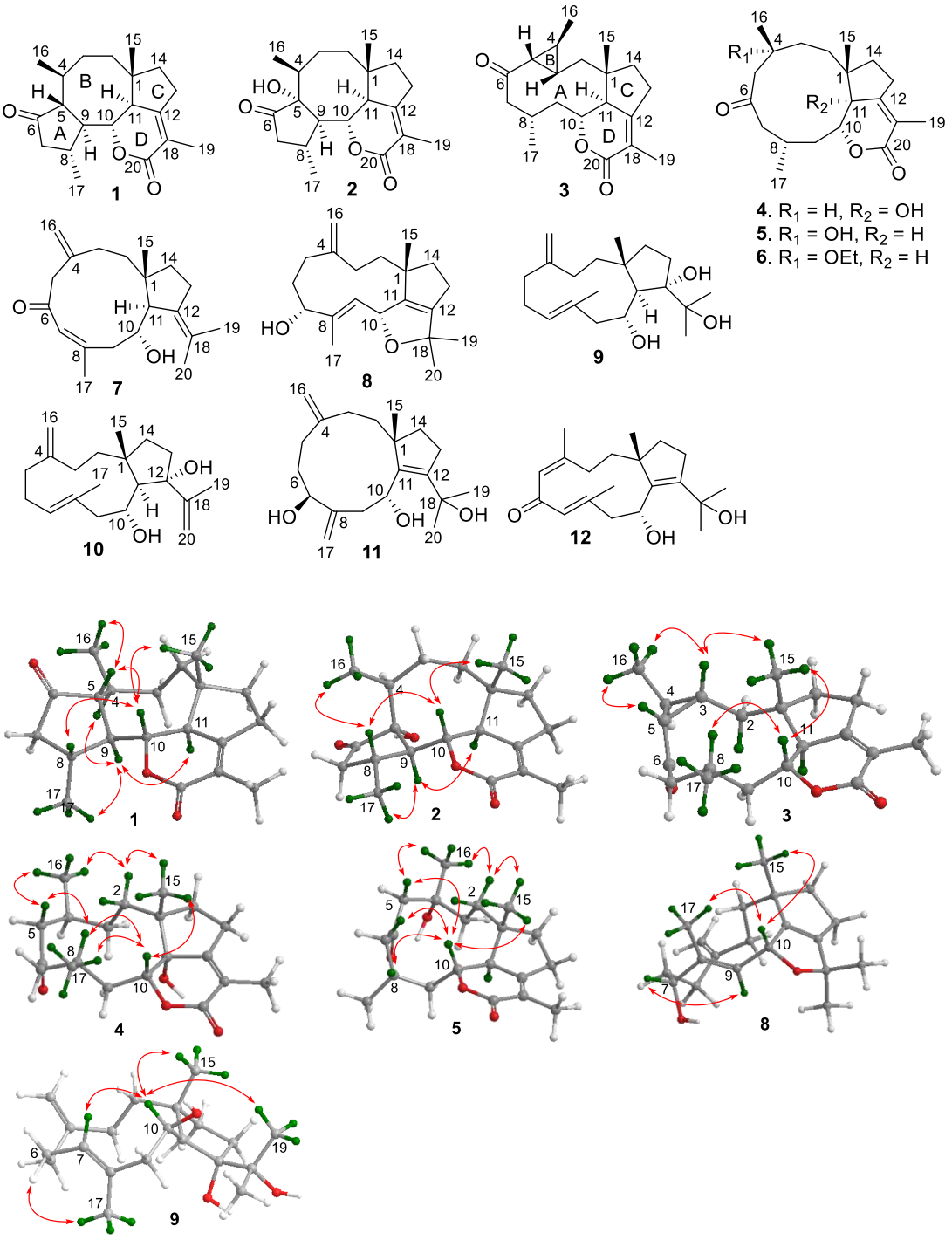

Figure 2. Key NOE correlations of **1**−**5** and **8**−**9**.

The relative configuration of **1** was determined by the key NOE data. The NOE correlations from H_3-15 to H-5 and H-10 and from H-10 to H-5 and H-8 (Figure 2) suggested the *trans*-fusions between rings A and B and between rings B and C with the same face of H-5 toward H-10 and H_3-15. The same orientations between H_3-17/H-9, H_3-16/H-5, and H-9/H-11 were evident from the relevant NOE relationships (Figure 2). The absolute configuration of **1** was determined by the X-ray diffraction employing graphite-monochromated Cu Kα radiation with a Flack parameter −0.04 (10) (Figure 3). Therefore, the stereogenic centers of **1** were assigned to 1*R*, 4*S*, 5*R*, 8*R*, 9*S*, 10*R*, and 11*S* configurations.

The molecular formula ($C_{20}H_{28}O_4$) of clavirolide K (**2**) was determined by the HRESIMS data, containing one more oxygen atom than that of **1**. Comprehensive analysis of 1D and 2D NMR data revealed that the structure of **2** closely resembled that of **1**. The only difference was C-5 (δ_C 85.0), a nonprotonated carbon to replace the methine of **1**. The HMBC correlations from H_3-16 (δ_H 0.98, d, J = 7.2 Hz) to C-3 (δ_C 31.9), C-4 (δ_C 42.0), and C-5 suggested a hydroxylation at C-5. The NOE correlations from H-10 to H_3-15 and H-8 and between H-8/H_3-16 and H-9/H-11 suggested the *trans* fusion of rings B and C but the *cis* fusion of rings A and B, along with the *syn* orientation of OH-5 toward H-9 and H-11 (Figure 2).

https://doi.org/10.1021/acsomega.3c02429
ACS Omega 2023, 8, 21254−21264

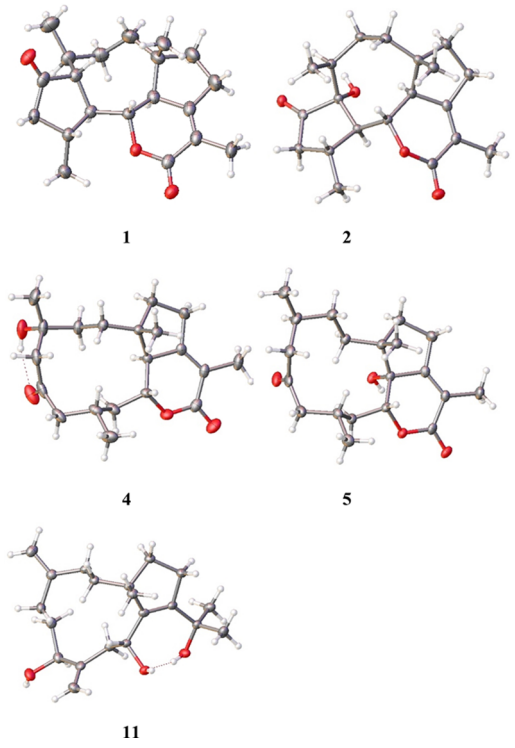

Figure 3. ORTEP views of the crystal structures of **1**−**2**, **4**−**5**, and **11**.

The X-ray diffraction data of single crystal were unambiguously determined to be 1*R*, 4*S*, 5*R*, 8*R*, 9*R*, 10*S*, and 11*S* for **2** (Figure 3).

Clavirolide L (**3**) has the same molecular formula as that of **1** as determined by the HRESIMS and NMR data. The NMR data of **3** resembled those of clavirolide C[17], suggesting the structural similarity. Diagnostic 1D and 2D NMR data clarified a dolabellane-type analogue with a tetracyclic ring system. The partial structure regarding cyclopentane (ring C) conjugated to an unsaturated α-methyl-δ-lactone (ring D) was identical to that of **1**. The COSY correlations from H-3 (δ_H 1.35, brddd, J = 4.8, 7.2, 8.0 Hz) to H_2-2 (δ_H 1.53, 2.04), H-4 (δ_H 1.50, m), and H-5 (δ_H 2.02) and between H-4 and H-5 suggested the presence of a cyclopropane unit (ring B), and this was supported by the HMBC correlations from H_3-16 (δ_H 1.11, d, J = 7.0 Hz) to C-3 (δ_C 31.5), C-4 (δ_C 19.7), and C-5 (δ_C 36.2). These findings in association with the COSY relationship between H_3-16 and H-4 clarified the substitution of a methyl group at C-4. The NOE interaction between H_3-15 and H-10 suggested the *trans*-fusion of rings A and C with the same orientation of H_3-15 toward H-10 (δ_H 4.27, dd). The NOE correlations of H_3-16 to H-3 and H-5 identified the same face of these groups. Additional NOE correlations between H_3-15/H-3 and H-8/H-10 were assigned the cofacial orientation of H-3 and H-8 toward H_3-15. The absolute configuration of **3** was determined by the comparison of the experimental ECD data with those calculated for the enantiomers of **3** by the TDDFT-ECD method (Figure 4A), suggesting the 1*S*, 3*S*, 4*S*, 5*R*, 8*S*, 10*R*, and 11*S* configurations.

Clavirolide M (**4**) has a molecular formula of $C_{20}H_{30}O_4$ on the basis of the HRESIMS data. The NMR data (Tables 1 and 2) of **4** were comparable to those of clavirolide C,[17] indicating a dolabellane-type analogue. The distinction was attributed to a hydroxylated C-11 (δ_C 79.1) instead of a methine carbon of clavirolide C due to the HMBC correlations from H_3-15 (δ_H 0.86, s) to C-1 (δ_C 47.8), C-2 (δ_C 31.6), C-11, and C-14 (δ_C 37.0). The relative configuration of **4** was identified by the NOE data, of which the NOE correlation between H_3-15 and H-10 suggested a *trans*-fusion of rings A and B with the same orientation of H-10 and H_3-15. The relative configurations of H_3-16 and H_3-17 were ambiguous due to the weak NOE correlations of the protons at stereogenic centers. Fortunately, the X-ray diffraction data with a Flack parameter −0.03 (7) helped to clarify the absolute configurations as 1*R*, 4*S*, 8*S*, 10*R*, and 11*R* (Figure 3).

The HRESIMS data showed the molecular formula of clavirolide N (**5**) to be the same as that of **4**, and the NMR data (Tables 1 and 2) of both compounds were very similar. The difference was C-4 (δ_C 73.7) and C-11 (δ_C 51.4) of **5** replacing C-4 (δ_C 31.2) and C-11 (δ_C 79.1) of **4**, suggesting the OH-11 of **4** to be shifted to C-4 of **5**. Thus, **5** is an isomer of **4** with an alternative substitution of the hydroxy group. The absolute configuration of **5** was elucidated by the X-ray

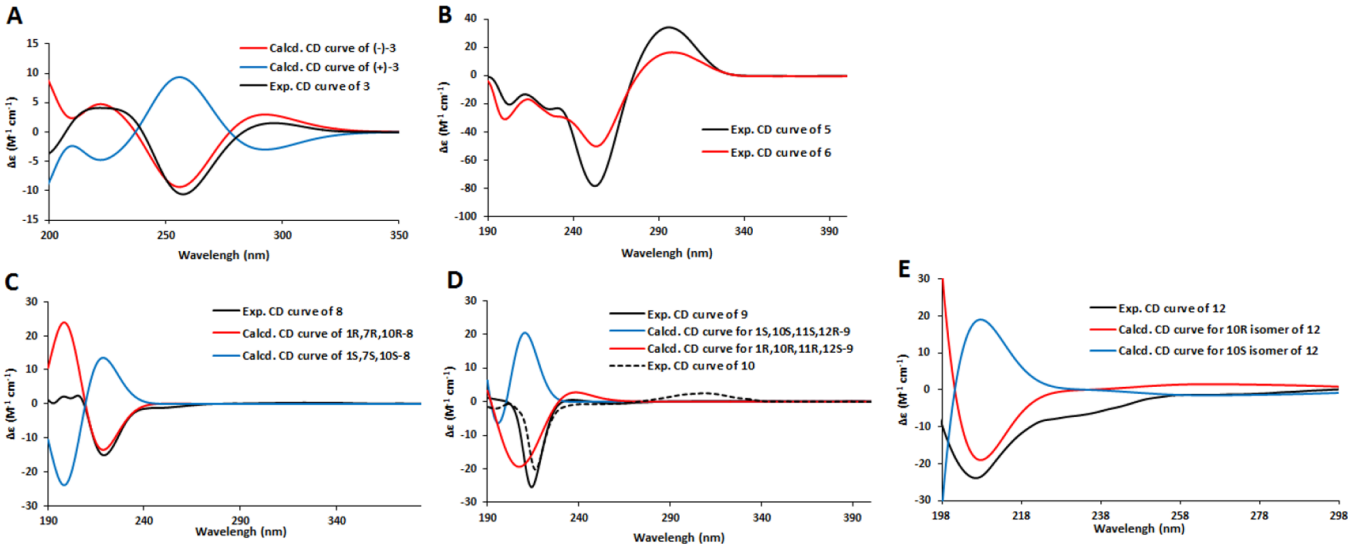

Figure 4. Experimental and calculated ECD data of **3**, **5**−**6**, **8**−**9**, and **12**.

https://doi.org/10.1021/acsomega.3c02429
ACS Omega 2023, 8, 21254−21264

Table 1. ^{1}H NMR Data of 1−6 ($CDCl_3$, δ (ppm), J (Hz))

no.	1	2	3	4	5	6
2	1.68, m	1.67, m	1.53, dd (4.8,15.6)	1.22, m	1.58, m	1.67, m
	1.70, m	1.70, m	2.04, brd (15.6)	1.58, m	1.60, m	1.70, m
3	1.55, m	1.50, m	1.35, brddd (4.8,7.2,8.0)	1.02, m	1.45, m	1.31, m
	1.93, m	1.90, m		1.43, m	1.60, m	1.67, m
4	1.74, m	1.90, m	1.50, m	2.23, m		
5	1.73, m		2.02, m	2.21, t (12.0)	3.12, d (16.1)	2.33, d (15.6)
				2.38, dd (3.0, 12.0)	2.26, d (16.1)	3.15, d (15.6)
7	2.09, dd (12.0,15.8)	2.04, dd (9.4,20.2)	2.69, dd (3.2,14.0)	2.23, dd (11.0, 12.0)	2.02, dd (10.8,11.4)	2.60, dd (3.0, 11.2)
	2.39, dd (3.0, 15.8)	2.74, dd (9.0,20.2)	2.22, dd (12.0,14.0)	2.42, dd (4.0, 12.0)	2.60, dd (2.8,10.8)	1.97, t (11.2)
8	2.23, m	2.38, m	2.37, m	2.07, m	2.18, m	2.29, m
9	2.02, ddd (6.2,8.0,10.0)	2.24, dd (9.0,11.4)	1.98, m	1.42, m	1.71, dd (12.0,15.2)	1.90, dd (9.0,14.8)
			1.83, m	2.41, m	1.98, dd (9.4,15.2)	1.67, m
10	4.02, dd (10.0, 11.4)	4.85, dd (10.0,11.4)	4.27, ddd (1,2,6.9,10.1)	4.35, ddd (2.2,6.0)	4.23,t (12.0)	4.22, t (10,1)
11	2.70, d (11.4)	3.24, d (10.0)	2.20, d (10.1)		2.61, d (12.0)	2.54, d (10.1)
13	2.42, m	2.41, m	2.40, m	2.51, m	2.46, m	2.41, m
	2.46, m	2.45, m	2.42, m	2.55, m	2.50, m	2.43, m
14	1.68, m;	1.60, m	1.68, m	1.60, m	1.45, m	1.83, m
	1.70, m	1.70, m	1.70, m	2.10, m	1.86, m	1.43, ddd (1.4,8.4,12.6)
15	0.98, s	0.89, s	0.99, s	0.86, s	0.91, s	0.91, s
16	1.06, d (6.2)	0.98, d (7.2)	1.11, d (6.0)	1.03, d (6.7)	1.19, s	1.53, s
17	1.42, d (7.0)	1.42, d (6.4)	1.23, d (6.7)	1.23, d (6.4)	1.17, d (6.4)	1.12, d (6.4)
19	1.84, s	1.84, brs	1.82, brs	1.85, brs	1.83, brs	1.82, brs
EtO						1.16, t (7.0)
						3.30, dq (7.0,12.0)
						3.39, dq (7.0, 12.0)

Table 2. ^{13}C NMR Data of Compounds 1−6 ($CDCl_3$, δ (ppm))

no.	1	2	3	4	5	6
1	44.2	44.0	43.5	47.8	45.0	44.8
2	34.0	34.0	36.7	31.6	34.8	32.3
3	31.3	31.9	31.5	32.7	34.9	29.9
4	37.1	42.0	19.7	31.2	73.7	76.3
5	54.0	83.0	36.2	50.8	47.7	48.0
6	217.5	220.2	209.1	211.6	215.2	210.0
7	47.0	44.6	52.2	52.6	53.9	54.8
8	33.3	32.0	30.4	29.7	26.4	26.2
9	54.4	62.0	40.3	36.6	43.2	43.0
10	83.8	80.0	79.8	81.1	77.5	77.7
11	53.5	46.7	55.3	79.1	51.4	51.4
12	161.6	159.0	161.9	160.9	160.3	160.8
13	27.3	26.3	26.9	26.4	27.0	27.0
14	44.1	44.1	43.1	37.0	36.8	36.7
15	23.1	20.2	19.5	21.5	23.7	23.7
16	18.2	18.7	17.6	22.2	27.3	25.4
17	23.7	22.6	22.8	22.6	21.6	21.6
18	120.3	117.8	120.0	121.6	120.1	120.0
19	12.5	12.3	12.7	12.6	12.4	12.4
20	165.6	164.5	166.2	165.8	165.9	166.1
EtO						15.8
						55.7

diffraction data with a Flack parameter −0.01 (5), revealing the 1*S*, 4*R*, 8*S*, 10*R*, and 11*S* configurations (Figure 3).

The structure of clavirolide O (**6**) was determined as an 4-ethoxy analogue of **5** based on the similar NMR data (Tables 1 and 2) of both analogues, except for the presence of an ethoxy group that was located at C-4 (δ_C 76.3) on the basis of the HMBC correlation between the EtO methylene protons (δ_H 3.30, 3.39) and C-4. The comparable NOE and ECD data suggested both **5** and **6** having the same configuration (Figure 4B). Because compound **6** in the acetone extract of the fresh sample was undetectable by the LC−MS/MS data, the EtO group in **6** was suspected to be derived by the EtOH extraction process.

The HRESIMS data established the molecular formula $C_{20}H_{30}O_2$ of clavirolide P (**7**), requiring six degrees of unsaturation. The IR absorptions at 3200 and 1700 cm^{-1} suggested the presence of hydroxy and carbonyl groups. The ^{13}C NMR data (Table 4) exhibited a total of 20 carbon resonances, and the DEPT classified them into one ketone, six olefinic resonances for three double bonds, four methyls, as well as the sp^3 resonances for six methylenes, two methines, and one nonprotonated carbon. These data together with the ^{1}H NMR resonances (Table 3) featured a dolabellane-type diterpene with a bicyclic scaffold, structurally related to dolabellanone-4.[19] A double bond that resided at C-12 (δ_C 136.1) and C-18 (δ_C 130.4) was characterized by the simultaneous HMBC correlations of the geminal methyl groups H_3-19 (δ_H 1.60, s) and H_3-20 (δ_H 1.70, s) to C-12 and C-18. The COSY correlations between H_2-13 (δ_H 2.20, 2.34) and H_2-14 (δ_H 1.40, 1.70), along with the HMBC correlations from H_3-15 (δ_H 1.00, s) to C-1 (δ_C 45.1), C-11, (δ_C 49.1) and C-14 (δ_C 40.0) and from H-11 (δ_H 2.95, d, J = 10.0 Hz) to C-12 and C-18, were indicative of a cyclopentane unit with the substitution of a methyl group at C-1. The COSY correlations assigned the alkyl subunits of H_2-2/H_2-3 and H_2-9/H-10 (δ_H 3.62, dt, J = 4.5, 10.0 Hz). The HMBC correlations of H_2-16 (δ_H 5.08, brs; 4.97, brs) to C-3 (δ_C 28.3) and C-5 (δ_C 55.9) and H_2-5 (δ_H 2.95, 3.38) and olefinic singlet H-7 (δ_H 6.35, s) to C-6 (δ_C 203.0), as well as H_3-17 (δ_H 2.06, s) to C-7 (δ_C 130.3), C-8 (δ_C 153.0), and C-9 (δ_C 36.0), assembled a cycloundecenone, in which a 6-ketone, a 4-*exo*-methylene (δ_C 143.6), a $\Delta^{7,8}$, an OH-10, and a methyl group at

https://doi.org/10.1021/acsomega.3c02429
ACS Omega 2023, 8, 21254−21264

Table 3. ^{1}H NMR Data of 7−12 ($CDCl_3$, δ (ppm), J (Hz))

no.	7	8	9	10	11	12
2	1.12, dt (6.4, 12.0)	1.35, m	1.35, m	1.32, m	1.35 ddd (4.0,7.0,12.0)	1.12. dt (2.0, 12.0)
	1.80, t (12.0)	1.70, dt (4.4,14.0)	1.37, m	1.60, m	1.50, dt (3.0, 12.0)	1.60, dt (4.0, 12.0)
3	2.15 dd (6.4,12.0)	1.95, m	1.91, dt (3.0, 12.0)	2.05, m	1.82, m	1.82, m
	2.30, t (12.0)	2.15, m	2.10, m	2.15, m	2.10, m	2.95, t (12.0)
5	2.95, d (11.0)	2.00, m	2.25, m	2.30, m	2.13, m	6.06, s
	3.38, d (11.0)	2.02, m	2.31, m	2.33, m	2.14, m	
6		1.80, dt (5.0, 12.0)	2.15, m	2.20, m	1.70, dq (5.0, 12.0)	
		1.88, m	2.25, m	2.21, m	1.90, m	
7	6.35, s	4.87, dd (5.0, 11.0)	5.35, t (6.0)	5.38, dd (2.0, 4.0)	4.35, dd (4.0,6.0)	5.88, s
9	2.20, m	5.09, d (9.2)	2.30, d (12.0)	2.34, m	2.55, dd (4.8, 13.0)	2.49, dd (3.0, 12.0)
	2.35, m		2.46, t (12.0)	2.35, m	2.73, dd (4.0, 13.0)	3.43, t (12.0)
10	3.62, dt (4.5, 10.0)	5.28, dd (2.8,9.2)	3.78,dd (3.0, 12.0)	4.91, ddd (4.0,6.0,10.0)	4.38, dd (4.0,4.8)	4.22, dd (3.0, 12.0)
11	2.95, d (10.0)		2.25, d (3.0)	2.36, d (10.0)		
13	2.20, m	2.00, m	1.57, m	1.52, m	2.25, m	1.82, m
	2.34, m	2.35, m	2.15, m	2.20, m	2.30, m	2.98, t (10.0)
14	1.40, m;	2.00, m	1.25, m	1.40, m	1.55, m	1.65, m
	1.70, m	2.05, m	1.57, m	1.85, m	1.82, m	1.81, m
15	1.00, s	1.05, s	0.94, s	1.03, s	1.10, s	1.20, s
16	4.95, brs; 5.10, brs	4.70, brs; 4.74, brs	4.69, brs; 4.74, brs	4.71, brs; 4.75, brs	4.67, brs; 4.71, brs	1.94, s
17	2.06, s	1.66, s	1.74, s	1.77, s	5.32, brs; 5.37, brs	1.81, s
19	1.60, s	1.17, s	1.41, s	2.02, brs	1.40, s	1.48, s
20	1.70, s	1.23, s	1.44, s	5.12, brs; 5.38, brs	1.40, s	1.50, s

C-8, respectively, were clarified. The NOE correlation between H_3-15 and H-10 deduced the *trans*-fusion of both rings, and the NOE correlation between H_3-17 and H-7 together with the chemical shift of C-17 (δ_C 28.3, >20 ppm) suggested a 7*Z* conformer.[21]

The molecular formula of clavirolide Q (**8**) was determined as $C_{20}H_{30}O_2$ with six degrees of unsaturation. The NMR data (Tables 3 and 4) featured a dolabellane-type diterpene, closely related to those of clavufuranolide C.[18] The presence of six olefinic resonances for three double bonds along with the remaining carbons for sp^3 resonances suggested a tricyclic structure. The locations of double bonds at C-4 (δ_C 150.2)/C-16 (δ_C 109.4), C-8 (δ_C 135.2)/C-9 (δ_C 132.5), and C-11 (δ_C 150.7)/C-12 (δ_C 149.0), respectively, were deduced by the HMBC correlations of the *exo*-methylene protons H_2-16 (δ_H 4.70, 4.74) to C-3 (δ_C 34.5), C-4, and C-5 (δ_C 30.6); H_3-17 (δ_H 1.66, s) to C-7 (δ_C 66.6), C-8, and C-9; and H-10 (δ_H 5.28, dd, J = 2.8, 9.2 Hz) to C-11 and C-12. An oxyisopropane unit at C-12 was evident from the simultaneous HMBC correlations of H_3-19 (δ_H 1.17, s)/H_3-20 (δ_H 1.23, s) to C-12 and C-18 (δ_C 81.4). In addition, the COSY correlations between H-9 (δ_H 5.09, d, J = 9.2 Hz)/H-10 (δ_H 5.28, dd, J = 2.8, 9.2 Hz) and H_2-6 (δ_H 1.80, 1.88)/H-7 (4.87, dd, J = 5.0, 11.0 Hz) along with the chemical shift of C-7 (δ_C 66.6) suggested a 7-hydroxylation. The HMBC correlation between H-10 and C-18 indicated an ether bond across the bridgeheads of C-10 (δ_C 75.2) and C-18. The $J_{H\text{-}9/H\text{-}10}$ value (9.2 Hz) suggested a *trans*-orientation between H-9 and H-10. The NOE correlations from H-10 to H_3-15 (δ_H 1.05, s) and H_3-17 suggested the same face of H-10 toward H_3-15 and 8*E* conformer. Comparison of the experimental and calculated ECD data (Figure 4C) suggested an *R* configuration for C-1 and C-10.

Table 4. ^{13}C NMR Data of Compounds 7−12 ($CDCl_3$, δ (ppm))

no.	7	8	9	10	11	12
1	45.1	45.1	45.0	43.6	52.3	51.4
2	38.3	34.8	37.1	38.8	38.4	39.5
3	28.3	34.5	30.2	30.5	30.2	31.2
4	143.6	150.2	151.9	151.7	149.9	160.0
5	55.9	30.6	35.8	36.1	28.0	129.9
6	203.0	33.5	28.6	28.3	31.4	199.0
7	130.3	66.6	129.3	130.2	73.0	128.9
8	153.0	135.2	131.4	131.4	149.9	139.0
9	36.0	132.5	47.4	47.0	42.1	48.9
10	68.0	75.2	70.3	71.3	68.8	65.8
11	49.1	150.7	57.7	56.9	142.6	140.5
12	136.1	149.0	90.1	86.3	144.3	145.5
13	27.4	23.2	36.9	38.9	33.9	34.4
14	40.0	46.9	32.5	35.2	33.8	35.2
15	19.8	21.2	23.7	24.9	28.1	29.6
16	115.0	109.4	111.0	111.8	111.4	26.6
17	28.3	16.8	18.6	18.1	109.7	19.2
18	130.4	81.4	75.0	152.6	72.7	74.0
19	21.2	27.2	26.7	22.1	29.9	30.1
20	22.1	27.2	27.0	113.0	30.9	31.8

The planar structure of clavirolide R (**9**) was identical to that of clavurol F[18] based on the 2D NMR and MS data. A 7*E* conformer of **9** as the case of the known analogue was evident from the NOE correlation between H-7 (δ_H 5.35, t, J = 6.0 Hz) and H_2-9 (δ_H 2.30, 2.46) and the chemical shift of C-17 (δ_C 18.6 < 20 ppm),[21] and the NOE interaction between H_3-15 (δ_H 0.94, s) and H-10 (δ_H 3.78, dd, J = 3.0, 12.0 Hz) suggested the same face of both groups and the *trans*-fusion of rings A and B. However, the distinctive ^{13}C NMR resonances at C-1 (δ_C 45.0 *vs* 43.5), C-11 (δ_C 57.7 *vs* 47.5), and C-15 (δ_C 23.7 *vs* 28.6) suggested **9** to be a stereoisomer of clavurol F. The observation of the NOE correlation between H-10 and H_3-19/H_3-20 suggested **9** to be a 12-isomer of clavurol F, and the $\Delta\delta^{R\text{-}S}$ values of the (*R*)- and (*S*)-MPA esters of **9** formed by the modified Mosher reaction[19,20] identified a 10*R* config-

https://doi.org/10.1021/acsomega.3c02429
ACS Omega 2023, 8, 21254−21264

uration (Figure 5). These together with the ECD data supported **9** to be a 12-epimer of clavurol F (Figure 4D).

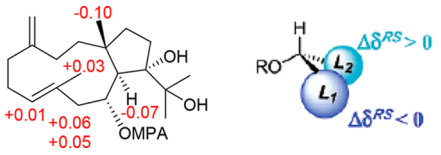

Figure 5. The $\Delta\delta^{R\text{-}S}$ values of the MPA esters of **9**.

Clavirolide S (**10**) has a molecular formula of $C_{20}H_{32}O_3$ as determined by the HRESIMS data, indicating five degrees of unsaturation. The NMR data (Tables 3 and 4) resembled those of **9**, with the sole difference of the substitution at C-12 (δ_C 86.3) by an isopropene unit as identified by the HMBC correlations of H_3-19 (δ_H 2.02, s) to C-18 (δ_C 152.6) and C-20 (δ_C 113) and of H_2-20 (δ_H 5.12, 5.38) to C-19 (δ_C 22.1) and C-12. The similar NOE and ECD data suggested **10** to be an 18,20-dehydrated product of **9** (Figure 4D).

The molecular formula ($C_{20}H_{32}O_3$) of clavirolide T (**11**) was determined by the HRESIMS data, and the NMR data featured a dolabellane-type diterpene, structurally related to clavudiol A.[22,23] The distinction was recognized by a $\Delta^{8,17}$ instead of a $\Delta^{7,8}$ as evidenced by the HMBC correlations of H_2-17 (δ_H 4.67, 4.71) to C-7 (δ_C 73.0) and C-9 (δ_C 42.1), and this finding also suggested a hydroxylation at C-7. The NOE interaction between H-10 and H_3-15 suggested the same orientation of both groups. The absolute configuration was identified by the X-ray diffraction of the single crystal with a Flack parameter of 0.0 (2), suggesting 1*R*, 7*S*, and 10*R* configurations.

Clavirolide U (**12**) was determined as a homologue of **11** based on the NMR data. With the exception of the identical cyclopentene moiety for both **11** and **12**, a dienone unit that resided at C-4 (δ_C 160.0)/C-5 (δ_C 129.9) and C-7 (δ_C 128.9)/C-8 (δ_C 139.0) with a ketone group at C-6 (δ_C 199.0) was identified by the HMBC correlations from H_3-16 (δ_H 1.94, s) to C-3, C-4, and C-5; H_3-17 (δ_H 1.81, s) to C-7, C-8, and C-9; and both olefinic protons H-5 (δ_H 6.06, s) and H-7 (δ_H 5.88, s) to C-6. The hydroxylation at C-10 was deduced by the COSY relationship from H_2-9 (δ_H 2.49, 3.43) to H-10 (δ_H 4.22, dd, J = 3.0, 12.0 Hz) and the HSQC correlation between H-10 and C-10 (δ_C 65.8), in association with the HMBC correlations from H-10 to C-1 (δ_C 51.4), C-11 (δ_C 140.5), and C-12 (δ_C 145.5). The NOE correlations of H_3-16/H-5 and H-7/H_2-9 suggested 4*Z* and 7*E* conformers, and the additional NOE correlation between H-10 (δ_H 4.22, dd, J = 3.0, 12.0 Hz) and H_3-15 (δ_H 0.91, s) clarified them to be in the same orientation. Comparison of the experimental ECD data with those computed for the 10*R* and 10*S* isomers of **12** supposed a 10*R* configuration (Figure 4E).

Clavinflols B and C were isolated and characterized as chlorinated dolabellanes.[20] Clavinflol C was automatically converted to an undescribed product, namely, clavirolide V (**13**) (Scheme 1), whose structure was identified by extensive spectroscopic data (Supporting Information). Clavinflol B was partially converted to clavinflol C in the $CDCl_3$ solution for a week. These findings suggest that relevant analogues with etherification or olefinic rearrangement may be generated by a nonenzymatic reaction.

Biogenetically, geranylgeranyl pyrophosphate is well recognized as a precursor, which follows the formation of an unusual *trans* bicycle [9,3,0] tetradecane nucleus with an efficient stereocontrolled transannular manner.[9] This postulation is proven by all coral-derived dolabellanes with a *trans*-fusion of the bicyclic nucleus. The co-isolated clavurol C[18] is considered as a parent molecule to connect the relevant analogues. It follows epoxidation, hydration, dehydration, olefinic rearrangement, etherification, chloration, and/or hydrogenation to generate the isolated analogues (Scheme 2).

Dolabelladienetriol is structurally related to the isolated dolabellanes, and it is a typical noncompetitive inhibitor of HIV-1 reverse transcriptase enzyme.[10,24] Oxidated derivatives showed stronger effects than dolabelladientriol.[25] The low cytotoxicity and high antiviral activity suggest that dolabellanes are potential leads for further anti-HIV investigation. These findings evoked our interest to detect the anti-HIV activities of the isolated analogues. Prior to the antiviral detection, all analogues were tested for cytotoxicity by the MTT method and showed no cytotoxicity toward tumor cell lines including A549, MCF-7, SMMC-7721, Hela, HCT-8, and MGC-803 at 100 μM. The *in vitro* anti-HIV-1 activities of the analogues were evaluated on vesicular stomatitis virus envelope glycoprotein G (VSV-G)-pseudotyped HIV-1-infected SupT1 cells with a firefly luciferase reporter gene. Clavirolide L (**3**) and clavirolide G displayed significant HIV-1 inhibition with more effects than the remaining analogues. For the analogues with unsaturated δ-lactone, clavirolide I, a 7,8-epoxide analogue of clavirolide G, attenuated the inhibitory effect; clavularinlide A, an analogue of clavirolide G with hydrogenated $\Delta^{7,8}$ but a $\Delta^{4,5}$ and 6,13-dione, decreased the activity. Clavirolide D, a 13-deoxidazed clavularinlide A, totally lost the activity, but clavirolide F (11-hydroxyclavirolide D) slightly improved the activity. Clavirolides M−O (**4**−**6**) with hydrogenated $\Delta^{4,5}$ but a 4-OH or 4-EtO unit of clavularinlide A showed weaker effects than clavularinlide A. These findings together with the data for clavirolides B−F and clavulactone suggested that a $\Delta^{7,8}$ group as the case of clavirolide G is necessary to improve the antiviral activity, except for clavirolide L (**3**) with a cyclopropane unit showing similar activity as clavirolide G (Table 5). Although dolabelladienetriol is reported as a potent inhibitor of the HIV-1 replication in primary cells *in vitro* through the inhibition of the enzyme RT,[10] the structurally related analogues such as clavirolides S and T, clauvdiols A and B, and clavirolide V showed weak to no activities, and all analogues weakly inhibited RT enzyme, suggesting that the mechanism of clavirolide L and clavirolide

Scheme 1. Conversion of Clavinflol B to 13 *via* Clavinflol C

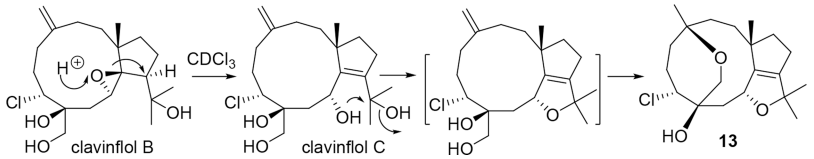

https://doi.org/10.1021/acsomega.3c02429
ACS Omega 2023, 8, 21254−21264

Scheme 2. Biogenetic Relationships of 1−12

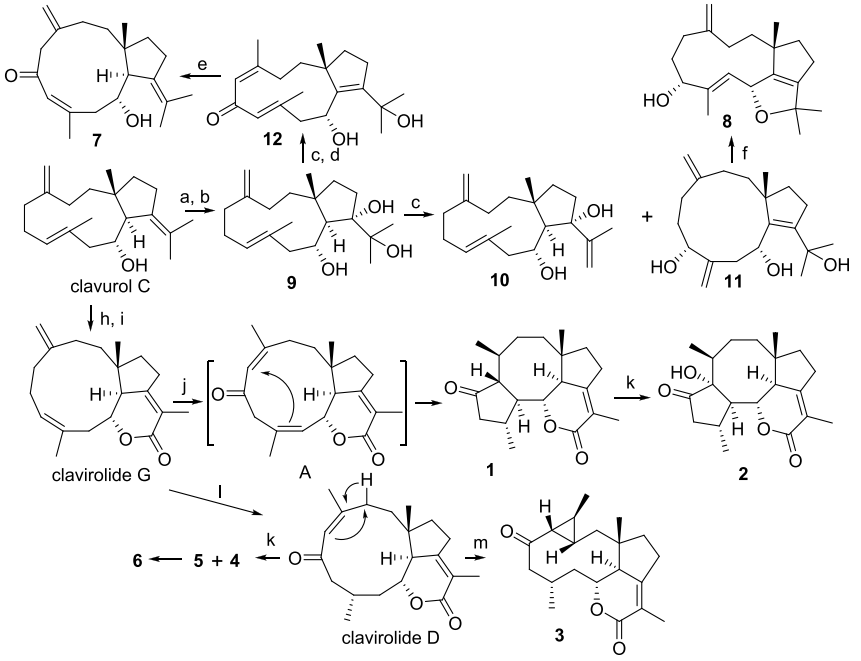

Table 5. Effects of Compounds on HIV-1 Inhibition

compounds	names	inhibition rate % (anti-HIV-1) 10 μM	IR % (anti-RT activity) 100 μM
1	clavirolide J (**1**)	32.05 ± 1.32	0
2	clavirolide K (**2**)	0	0
3	clavirolide M (**4**)	0	9.01 ± 7.6
4	clavirolide N (**5**)	0	26.63 ± 7.05
5	clavirolide O (**6**)	22.5 ± 3.55	32.64 ± 7.52
6	clavirolide F	23.08 ± 15.15	5.3 ± 4.2
7	clavularinlide A	30.37 ± 5.15	15.19 ± 11.18
8	clavirolide L (**3**)	62.56 ± 2.8	0
9	clavirolide I	20.56 ± 5.89	0
10	clavirolide G	64.25 ± 5.65	0
11	clavirolide D	0	0
12	clavirolide B	0	0
13	clavulactone	0	0
14	clavirolide C	0	0
15	clavirolide E	0	0
16	clavirolide F	0	0
17	clavirolide R (**9**)	30.73 ± 14.19	0
18	clavirolide T (**11**)	0	0
20	clavirolide S (**10**)	37.56 ± 17.25	0
21	clauvdiol A	0	0
22	clavudiol B	0	0
23	clavirolide U (**12**)	0	0
EFV		95.79 ± 0.38	96.87 ± 0.44

G was unrelated to RT enzyme and differed from efavirenz (EFV). The detailed mechanism remains elusive.

CONCLUSIONS

In the present study, an LC−MS/MS-guided fractionation of the soft coral *C. viridis* resulted in the isolation of 12 new dolabellane diterpenoids. Their structures were characterized by extensive analyses of the spectroscopic data, including the ECD and X-ray diffraction data for the configurational assignments. Clavirolides J and K (**1** and **2**) possessing an unsaturated δ-lactone bearing a tetracyclic scaffold are uncommonly found in the dolabellane family, and clavirolide L (**3**) with a cycloprotane-bearing tetracyclic moiety is unique in nature. These findings enriched the scaffold diversity of dolabellanes. The automatic conversion of clavinflol B to clavirolide V *via* clavinflol C suggests that some analogues with ether or olefinic groups may be artifacts rather than originating from the host. Clavirolide L and clavirolide G showed significant inhibition against HIV-1 without RT enzyme inhibition, providing additional non-nucleosides with different mechanisms from efavirenz. The mode of action remains for further investigation.

EXPERIMENTAL SECTION

General Methods. Optical rotations were detected by an Autopol III automatic polarimeter (Rudolph Research Co., Ltd.). UV spectra were recorded by a Cary 300 spectrometer. IR spectra were measured by a Thermo Nicolet Nexus 470 FT-IR spectrometer. ECD spectra were obtained by a JASCO-815 CD spectrometer. The ^{1}H and ^{13}C NMR spectra were acquired by a Bruker Advance 400. HRESIMS spectra were detected by an Autospee Ultima-TFO spectrometer. Silica gels with the size of 200−300 mesh (Qingdao Marine Chemistry Co. Ltd.), ODS (C_{18}, 10 μm, YMC), and Sephadex LH-20 (18−110 μm, Pharmacia) were utilized for chromatographic separation. An Alltech instrument (426-HPLC pump) linked to an Alltech UVIS-200 detector and associated with a Prevail C_{18} column (semipreparative, 5 μm) was used for semi-preparative HPLC separation.

https://doi.org/10.1021/acsomega.3c02429
ACS Omega 2023, 8, 21254−21264

Marine Soft Coral. Soft coral *Clavularia viridis* was collected from the Yongxing island of Xisha, South China Sea, in May of 2017. The coral samples were frozen immediately after collection. The specimen coded XSA-115 was identified by Prof. Leen van Ofwegen (National Museum of National History Naturalis) and was deposited at the State Key Laboratory of Natural and Biomimetic Drugs, Peking University.

UPLC−ESI-MS/MS Detection and Molecular Networking. A Thermo Vanquish F UPLC system coupled to the Thermo Q Exactive HF-X mass spectrometer with an electrospray ionization (ESI) source at a mass range of *m/z* 200−800 Da was used to detect the metabolite profile of the EtOAc extract. The Thermo Xcalibur Qual Browser software was applied for the extraction and analyses of the TIC and EIC spectra. The parameters (source voltage 3.5 kV, lens 1 voltage −10 V, capillary temperature 320 °C, gate lens voltage −40 V, capillary voltage 40 V, and tube lens voltage 100 V) were optimized. UPLC−MS/MS data were converted to .mzXML and .mgf format with MS-Convert, whereas data preprocessing and filtering were conducted using MZmine-2.53 and Python 3.8.5. The filtered fragment ion was set as 165.09 ± 0.05 Da. The prepared data were uploaded and analyzed on the GNPS platform (https://gnps.ucsd.edu/ProteoSAFe/static/gnps-splash.jsp). Parameters of molecular network were established to keep the precursor and product ion mass tolerance under 0.05 Da. To generate molecular networks, six minimum matched peaks and a cosine score of 0.70 were selected. Edges between nodes in the network were connected if the nodes at top-10 ranked nodes were considered. Data were visualized using the Cytoscape 3.8.2 software.

Extraction and Isolation. The homogenized soft coral *C. viridis* (1.6 kg) was extracted with 95% EtOH (2 L × 3) and then concentrated under a vacuum. The crude extract (32.0 g) was desalted in MeOH. The concentrated residue was further partitioned between H_2O and EtOAc. The EtOAc layer was detected by the LC−MS/MS method. Annotation of the molecular cluster of the networking established by the GNPS platform implied the EtOAc fraction containing dolabellane-related terpenes. The EtOAc fraction (18.5 g) was subjected to a silica gel (160−200 mesh, 350 g) column chromatography (8.5 × 60 cm) eluting with a gradient of petroleum ether (PE)/acetone (from 100:1 to 1:1) to yield eight fractions (FA−FH). ^{1}H NMR detection revealed fractions FC to FE showing terpene features. FC (5.0 g) was subjected to an ODS column eluting with MeOH-H_2O (8:2) to obtain clavularinlide B (10.3 mg), clavirolide G (172.4 mg), clavirolide F (6.4 mg), clavularinlide A (1.0 mg), clavirolide I (7.6 mg), clavirolide D (42.3 mg), clavirolide B (7.7 mg), clavulactone (19.8 mg), clavirolide C (200.7 mg), clavirolide E (28.9 mg), clavirolide F (6.4 mg), clauvdiol A (152.9 mg), and clauvdiol B (5.2 mg). FD (2.0 g) was chromatographed by semipreparative HPLC with acetonitrile-H_2O (6:4) to yield **1** (7.9 mg), **3** (2.4 mg), **4** (4.3 mg), **6** (17.2 mg), **7** (200.7 mg), **9** (42.3 mg), **11** (7.7 mg), and **12** (19.8 mg). FE (1.6 g) was separated on a semipreparative HPLC column with a mobile phase of MeOH-H_2O (6:4) to afford **8** (1.0 mg), **10** (6.4 mg), **2** (3.1 mg), and **5** (3.8 mg).

Clavirolide J (**1**): colorless crystal, mp 121.6−122.4°, $[\alpha]^{20}_D$ −53.0 (*c* 0.1, MeOH). IR (KBr) ν_{max} 2923, 1736, 1709 cm^{-1}; ^{1}H and ^{13}C NMR data, see Tables 1 and 2; HRESIMS *m/z* 317.2117 $[M + H]^+$ (calcd for $C_{20}H_{29}O_3$, 317.2117).

Clavirolide K (**2**): colorless crystal, mp 165.0−165.9°, $[\alpha]^{20}_D$ 52.0 (*c* 0.1, MeOH). IR (KBr) ν_{max} 3431, 2953, 1747, 1702 cm^{-1}; ^{1}H and ^{13}C NMR data, see Tables 1 and 2; HRESIMS *m/z* 333.2061 $[M + H]^+$ (calcd for $C_{20}H_{29}O_4$, 333.2066).

Clavirolide L (**3**): colorless oil, $[\alpha]^{20}_D$ −8.0 (c 0.1, MeOH). IR (KBr) ν_{max} 2954, 1705, 1684 cm^{-1}; ECD (*c* 0.02 MeOH) λ_{max} ($\Delta\varepsilon$) 222 (4.1), 258 (−10.6), 295 (1.5); ^{1}H and ^{13}C NMR data, see Tables 1 and 2; HRESIMS *m/z* 317.2111 $[M + H]^+$ (calcd for $C_{20}H_{29}O_3$, 317.2117).

Clavirolide M (**4**): colorless crystal, mp 138.4−139.0°, $[\alpha]^{20}_D$ 1.0 (*c* 0.1, MeOH). IR (KBr) ν_{max} 2953, 1693, 734 cm^{-1}; ECD (*c* 0.02 MeOH) λ_{max} ($\Delta\varepsilon$) 202 (26.3), 226 (−21.1); ^{1}H and ^{13}C NMR data, see Tables 1 and 2; HRESIMS *m/z* 333.2069 $[M - H]^-$ (calcd for $C_{20}H_{29}O_4$, 333.2066).

Clavirolide N (**5**): colorless crystal, mp 144.8−145.6°, $[\alpha]^{20}_D$ −10.0 (*c* 0.1, MeOH). IR (KBr) ν_{max} 2959, 1701 cm^{-1}; ^{1}H and ^{13}C NMR data, see Tables 1 and 2; HRESIMS *m/z* 335.2220 $[M + H]^-$ (calcd for $C_{20}H_{31}O_4$, 335.2222).

Clavirolide O (**6**): colorless oil, $[\alpha]^{20}_D$ −18.0 (*c* 0.1, MeOH). IR (KBr) ν_{max} 2959, 1703 cm^{-1}; ^{1}H and ^{13}C NMR data, see Tables 1 and 2; HRESIMS *m/z* 361.2374 $[M - H]^-$ (calcd for $C_{22}H_{33}O_4$, 361.2379).

Clavirolide P (**7**): colorless oil, $[\alpha]^{20}_D$ 40.0 (*c* 0.05, MeOH). IR (KBr) ν_{max} 2928, 1714, 1021 cm^{-1}; ^{1}H and ^{13}C NMR data, see Tables 3 and 4; HRESIMS *m/z* 303.1961 $[M + H]^+$ (calcd for $C_{20}H_{30}O_2$, 303.1960).

Clavirolide Q (**8**): colorless oil, $[\alpha]^{20}_D$ −13.3 (*c* 0.12, MeOH). IR (KBr) ν_{max} 3450, 2942, 1644, 1033 cm^{-1}; ECD (*c* 0.02, MeOH) λ_{max} ($\Delta\varepsilon$) 198 (23.9), 219 (−13.5); ^{1}H and ^{13}C NMR data, see Tables 3 and 4; HRESIMS *m/z* 320.2584 $[M + H]^+$ (calcd for $C_{20}H_{34}O_3$, 320.2590).

Clavirolide R (**9**): colorless oil, $[\alpha]^{20}_D$ −8.0 (*c* 0.1, MeOH). IR (KBr) ν_{max} 3260, 2930, 1381 cm^{-1}; ECD (*c* 0.02, MeOH) λ_{max} ($\Delta\varepsilon$) 207 (−19.4); ^{1}H and ^{13}C NMR data, see Tables 3 and 4; HRESIMS *m/z* 321.2433 $[M - H]^-$ (calcd for $C_{20}H_{34}O_3$, 321.2430).

Clavirolide S (**10**): colorless oil, $[\alpha]^{20}_D$ −100.0 (*c* 0.1, MeOH). IR (KBr) ν_{max} 2932, 1015 cm^{-1}; ^{1}H and ^{13}C NMR data, see Tables 3 and 4; HRESIMS *m/z* 303.2322 $[M - H]^-$ (calcd for $C_{20}H_{32}O_2$, 303.2324).

Clavirolide T (**11**): square crystal (MeOH-H_2O), mp 143.5−144.1°, $[\alpha]^{20}_D$ −10.0 (*c* 0.1, MeOH). IR (KBr) ν_{max} 3202, 2934 cm^{-1}; ^{1}H and ^{13}C NMR data, see Tables 3 and 4; HRESIMS *m/z* 319.2275 $[M - H]^-$ (calcd for $C_{20}H_{32}O_3$, 319.2273). Flack 0.0(2) (CCDC 2155823).

Clavirolide U (**12**): colorless oil, $[\alpha]^{20}_D$ −6.1 (*c* 0.065, MeOH). IR (KBr) ν_{max} 3376, 2979, 2930, 1707, 1623 cm^{-1}; ECD (*c* 0.02, MeOH) λ_{max} ($\Delta\varepsilon$) 205 (−38.6), 234 (10.5); ^{1}H and ^{13}C NMR data, see Tables 3 and 4; HRESIMS *m/z* 319.2275 $[M - H]^-$ (calcd for $C_{20}H_{32}O_3$, 319.2273).

Clavirolide V (**13**): colorless oil, $[\alpha]^{20}_D$ 26.0 (*c* 0.1, MeOH). IR (KBr) ν_{max} 2932, 1686 cm^{-1}; ECD (*c* 0.02, MeOH) λ_{max} ($\Delta\varepsilon$) 222 (−6.3); ^{1}H and ^{13}C NMR data, see Tables 3 and 4; HRESIMS *m/z* 372.2303 $[M + H]^+$ (calcd for $C_{20}H_{33}ClO_4$, 372.2305).

X-ray Crystallography Data. Colorless prisms were crystalized in EtOH solution, and the X-ray diffraction was performed on a Rigaku Micromax 002+ diffractometer with graphite monochromated Cu Kα radiation at 150 K, λ(Cu Kα) = 1.54184 Å.

https://doi.org/10.1021/acsomega.3c02429
ACS Omega 2023, 8, 21254−21264

The crystal of **1** (0.51 × 0.22 × 0.05 mm^3) belongs to the monoclinic system, space group $P2_1$, with a = 12.23050(10) Å, b = 16.56450(10) Å, c = 18.0244(2) Å, β = 109.3100(10)°, V = 3446.17(6) $Å^3$, Z = 8, D_{calcd} = 1.220 g/cm^3, μ(Cu Kα) = 0.633 mm^{-1}, and $F(000)$ = 1376.0. A total of 78,679 reflections were collected in the range of 7.45° ≤ 2θ ≤ 133.172°. The refined structural model converged to a final R_1 = 0.0589; wR_2 = 0.1450; goodness-of-fit on $F2$ = 1.030 for 11,741 observed reflections [$I > 2\sigma(I)$]. The absolute configuration of **1** was determined by the Flack parameter (zero for correct absolute configuration), which was refined against the data of Bijvoet pairs. The Flack parameter of **1** was −0.04(10).

The crystal of **2** (0.19 × 0.16 × 0.02 mm^3) belongs to the orthorhombic system, space group $P2_12_12_1$, with a = 6.62950(10) Å, b = 11.9660(3) Å, c = 21.4080(4) Å, V = 1698.27(6) $Å^3$, Z = 4, D_{calcd} = 1.300 g/cm^3, μ(Cu Kα) = 0.714 mm^{-1}, and $F(000)$ = 720.0. A total of 9442 reflections were collected in the range of 8.26° ≤ 2θ ≤ 153.896°. The refined structural model converged to a final R_1 = 0.0345; wR_2 = 0.0889; goodness-of-fit on $F2$ = 1.084 for 3347 observed reflections [$I > 2\sigma(I)$]. The Flack parameter was 0.00(9).

The crystal of **4** (0.12 × 0.04 × 0.02 mm^3) belongs to the monoclinic system, space group $P2_1$, with a = 8.67365(18) Å, b = 5.96828(12) Å, c = 18.1373(3) Å, β = 97.9165(18)°, V = 929.96(3) $Å^3$, Z = 2, D_{calcd} = 1.194 g/cm^3, μ(Cu Kα) = 0.652 mm^{-1}, $F(000)$ = 364.0. A total of 14,188 reflections were collected in the range 4.92° ≤ 2θ ≤ 154.372°. The refined structural model converged to a final R_1 = 0.0314; wR_2 = 0.0807; goodness-of-fit on $F2$ = 1.048 for 3747 observed reflections [$I > 2\sigma(I)$]. The Flack parameter was −0.03(7).

The crystal of **5** (0.12 × 0.01 × 0.01 mm^3) belongs to the monoclinic system, space group $P2_1$, with a = 9.06990(10) Å, b = 15.2150(2) Å, c = 21.4080(4) Å, β = 99.1830(10)°, V = 1840.08(4) $Å^3$, Z = 4, D_{calcd} = 1.240 g/cm^3, μ(Cu Kα) = 0.693 mm^{-1}, and $F(000)$ = 748.0. A total of 28,889 reflections were collected in 6.628° ≤ 2θ ≤ 148.994°. The refined structural model converged to a final R_1 = 0.0343; wR_2 = 0.0875; goodness-of-fit on $F2$ = 1.044 for 7204 observed reflections [$I > 2\sigma(I)$]. The Flack parameter was 0.01(5).

X-ray diffraction data of **11**: monoclinic crystal, space group $P2_12_12_1$, a = 7.8943(2) Å, b = 10.4660(3) Å, c = 21.7508(7) Å, α = 90°, β = 90°, γ = 90°, V = 1797.09(9) $Å^3$, Z = 4, T = 99.99(10) K, μ(Cu Kα) = 0.608 mm^{-1}, D_{calc} = 1.184 g/cm^3, and $F(000)$ = 704.0. A total of 11,037 reflections were collected in 8.12° ≤ 2θ ≤ 150.6°, and 3539 unique reflections (R_{int} = 0.0513, R_{sigma} = 0.0562) were used in all calculations. The refined structural model converged to a final R_1 = 0.0373 and wR_2 = 0.0911. Final R_1 = 0.0373 (>2sigma(I)) and wR_2 = 0.0939 (all data), goodness-of-fit on $F2$ = 1.055, and Flack = 0.0(2).

The structure was solved by direct methods (SHELXT) and refined by a full-matrix least-square procedure on F^2 values (SHELXL). The crystallographic data of **1**, **2**, **4**, **5**, and **11** were deposited in the Cambridge Crystallographic Data Centre (CCDC-2114825, CCDC-2114831, CCDC-2155480, CCDC-2114925, and CCDC-2155823).

ECD Calculation. Conformational random search was performed using the Sybyl-X 2.0 in the MMFF94S force field with 2.5 kcal/mol energy cutoff. Then, the GAUSSIAN 09 program was used to optimize the conformers under the DFT at the b3lyp/6-31 + g(d) level with MeOH as a solvent. Using the TDDFT method at the b3lyp/6-31 + g(d,p) level, the energies, oscillator strengths, and rotational strengths (velocity) of the first 30 electronic excitations were calculated. The computed ECD spectra were simulated by the overlapping Gaussian function, and the simulated ECD spectra were averaged by the Boltzmann distribution and the relative Gibbs free energy (ΔG). Calculated ECD spectra of the corresponding enantiomers were obtained by direct inversion of the ECD data computed for the model molecules. Comparison of the experimental and calculated ECD spectra allowed the depiction of the absolute configuration.

Mosher Method. To the CH_2Cl_2 (2.5 mL) solution of **9** (1.5 mg, 0.0046 mmol), (*R*)-MPA (1.2 mg, 0.0069 mmol), DCC (1.5 mg), and DMAP (0.06 mg) were added to stir at room temperature for 12 h. TLC detection was used to monitor the reaction. The (*R*)-MPA ester (1.1 mg, **9a**) was obtained after the purification by silica gel column chromatography eluting with acetone/PE = 1:3. The (*S*)-MPA ester (1.0 mg, **9b**) was yielded by the reaction of **9** (1.3 mg) with (*S*)-MPA using the same protocol as for **9a**.

$\Delta\delta$ (δ_R-δ_S) values: $\Delta\delta_{H\text{-}7}$ +0.01, $\Delta\delta_{H2-9}$ +0.05, +0.06, $\Delta\delta_{H3-17}$ +0.03, $\Delta\delta_{H\text{-}11}$ −0.07, $\Delta\delta_{H3-15}$ −0.10, $\Delta\delta_{H2-13}$ −0.01, and $\Delta\delta_{H2-14}$ −0.01.

In Vitro Anti-HIV Bioassay. To detect the inhibitory effects of compounds against HIV-1, HEK293T cells were cotransfected with 300 ng of pNL4-3Luc(R-E-) and 200 ng of 500 VSVG plasmid DNA in six-well plates. After incubation for 48 h, the supernatant was collected and filtered by a 0.45 μm filter to infect SupT1 cells (1 × 10^5) in 96-well plates. Each compound was added into the wells and incubated under 5% CO_2 at 37 °C for 48 h. After SupT1 cells were lysed, the firefly luciferase activities were detected by a firefly luciferase assay system (Promega) to calculate the inhibition rate.

In Vitro HIV-1 RT Activity Assay. To detect the activity of the compound against HIV-1 reverse transcriptase (RT) *in vitro*, a one-step real-time PCR assay using RT-PCR Kit (Takara, RR066A) was performed. The results were calculated by the $2^{-\triangle\triangle Ct}$ comparative method with DMSO as the blank control.

■ ASSOCIATED CONTENT

Supporting Information

The Supporting Information is available free of charge at https://pubs.acs.org/doi/10.1021/acsomega.3c02429.

IR, 1D and 2D NMR, and HRMS spectra of **1**−**13** (PDF)

■ AUTHOR INFORMATION

Corresponding Authors

Wei Cheng − *State Key Laboratory of Natural and Biomimetic Drugs, Ningbo Institute of Marine Medicine, Peking University, Beijing 100191, P.R. China;* orcid.org/0000-0002-5297-7046; Email: chengwei@bjmu.edu.cn

Wenhan Lin − *State Key Laboratory of Natural and Biomimetic Drugs, Ningbo Institute of Marine Medicine, Peking University, Beijing 100191, P.R. China;* orcid.org/0000-0002-4978-4083; Email: whlin@bjmu.edu.cn

Authors

Xin Dong − *State Key Laboratory of Natural and Biomimetic Drugs, Ningbo Institute of Marine Medicine, Peking University, Beijing 100191, P.R. China*

https://doi.org/10.1021/acsomega.3c02429
ACS Omega 2023, 8, 21254−21264

Jingshuai Wu − *State Key Laboratory of Natural and Biomimetic Drugs, Ningbo Institute of Marine Medicine, Peking University, Beijing 100191, P.R. China*
Hongli Jia − *State Key Laboratory of Natural and Biomimetic Drugs, Ningbo Institute of Marine Medicine, Peking University, Beijing 100191, P.R. China*
Shan Cen − *Key Laboratory of Antiviral Drug Research, Institute of Medicinal Biotechnology, Chinese Academy of Medical Sciences and Peking Union Medical College, Beijing 100050, P.R. China;* orcid.org/0000-0003-3358-0411

Complete contact information is available at: https://pubs.acs.org/10.1021/acsomega.3c02429

Author Contributions

[§]X.D. and J.W. contributed equally to this work.

Notes

The authors declare no competing financial interest.

■ ACKNOWLEDGMENTS

This work was supported by NSFC grants (81991525, 81991521) and COMRA DY135-B-05.

■ REFERENCES

(1) Zhang, L. T.; Wang, X. L.; Wang, T.; Zhang, J. S.; Huang, Z. Q.; Shen, T.; Lou, H. X.; Ren, D. M.; Wang, X. N. Dolabellane and clerodane diterpenoids from the twigs and leaves of *Casearia kurzii*. *J. Nat. Prod.* **2020**, *83*, 2817−2830.
(2) Antony, T.; Chakraborty, K.; Joy, M. Antioxidative dolabellanes and dolastanes from brown seaweed *Padina tetrastromatica* as dual inhibitors of starch digestive enzymes. *Nat. Prod. Res.* **2021**, *35*, 614−626.
(3) Yang, B.; He, Y.; Lin, S.; Zhang, J.; Li, H.; Wang, J.; Hu, Z.; Zhang, Y. Antimicrobial dolabellanes and atranones from a marine-derived strain of the toxigenic fungus *Stachybotrys chartarum*. *J. Nat. Prod.* **2019**, *82*, 1923−1929.
(4) Raldugin, V. A.; Shevtsov, S. A. Polycyclic diterpenoids biogenetically related to the cembranoids. *Chem. Nat. Compd.* **1987**, *23*, 269−281.
(5) Lei, H. Diterpenoids of gorgonian corals: chemistry and bioactivity. *Chem. Biodiversity* **2016**, *13*, 345−365.
(6) Hanif, N.; Murni, A.; Tanaka, J. Sangiangols A and B, two new dolabellanes from an Indonesian marine soft coral, *Anthelia sp*. *Molecules* **2020**, *25*, 3803−3812.
(7) Gao, Y.; Xiao, W.; Liu, H. C.; Wang, J. R.; Yao, L. G.; Ouyang, P. K.; Wang, D. C.; Guo, Y. W. Clavirolide G, a new rare dolabellane-type diterpenoid from the Xisha soft coral *Clavularia viridis*. *Chin. Chem. Lett.* **2017**, *28*, 905−908.
(8) Han, X.; Luo, X. C.; Xue, L.; van Ofwegen, L.; Zhang, W. J.; Liu, K. C.; Zhang, Y.; Tang, X. L.; Li, P. L.; Li, G. Q. Dolabellane diterpenes and elemane alkaloids from the soft coral *Clavularia inflata* collected in the South China Sea. *J. Nat. Prod.* **2022**, *85*, 276−283.
(9) Rodríguez, A. D.; González, E.; Ramírez, C. The structural chemistry, reactivity, and total synthesis of dolabellane diterpenes. *Tetrahedron* **1998**, *54*, 11683−11729.
(10) Cirne-Santos, C. C.; Souza, T. M. L.; Teixeira, V. L.; Fontes, C. F. L.; Rebello, M. A.; Castello-Branco, L. R. R.; Abreu, C. M.; Tanuri, A.; Frugulhetti, I. C. P. P.; Bou-Habib, D. C. The dolabellane diterpene Dolabelladienetriol is a typical noncompetitive inhibitor of HIV-1 reverse transcriptase enzyme. *Antiviral Res.* **2008**, *77*, 64−71.
(11) Wang, X.; Serrano, R.; González-Menéndez, V.; Mackenzie, T. A.; Ramos, M. C.; Frisvad, J. C.; Larsen, T. O. A Molecular Networking Based Discovery of Diketopiperazine Heterodimers and Aspergillicins from *Aspergillus caelatus*. *J. Nat. Prod.* **2022**, *85*, 25−33.
(12) Nothias, L.-F.; Nothias-Esposito, M.; da Silva, R.; Wang, M.; Protsyuk, I.; Zhang, Z.; Sarvepalli, A.; Leyssen, P.; Touboul, D.; Costa, J.; Paolini, J.; Alexandrov, T.; Litaudon, M.; Dorrestein, P. C. Bioactivity-Based Molecular Networking for the Discovery of Drug Leads in Natural Product Bioassay-Guided Fractionation. *J. Nat. Prod.* **2018**, *81*, 758−767.
(13) Hanke, W.; Patt, J.; Alenfelder, J.; Voss, J. H.; Zdouc, M. M.; Kehraus, S.; Kim, J. B.; Grujičić, G. V.; Namasivayam, V.; Reher, R.; Müller, C. E.; Kostenis, E.; Crüsemann, M.; König, G. M. Feature-Based Molecular Networking for the Targeted Identification of G_q-Inhibiting FR900359 Derivatives. *J. Nat. Prod.* **2021**, *84*, 1941−1953.
(14) Freire, V. F.; Gubiani, J. R.; Spencer, T. M.; Hajdu, E.; Ferreira, A. G.; Ferreira, D. A. S.; de Castro Levatti, E. V.; Burdette, J. E.; Camargo, C. H.; Tempone, A. G.; Berlinck, R. G. S. Feature-Based Molecular Networking Discovery of Bromopyrrole Alkaloids from the Marine Sponge *Agelas dispar*. *J. Nat. Prod.* **2022**, *85*, 1340−1350.
(15) Woo, S.; Kang, K. B.; Kim, J.; Sung, S. H. Molecular Networking Reveals the Chemical Diversity of Selaginellin Derivatives, Natural Phosphodiesterase-4 Inhibitors from *Selaginella tamariscina*. *J. Nat. Prod.* **2019**, *82*, 1820−1830.
(16) Sun, B.; Xu, X. General synthetic approach to bicyclo[9.3.0]-tetradecenone: a versatile intermediate to clavulactone and clavirolides. *Tetrahedron Lett.* **2005**, *46*, 8431−8434.
(17) Su, J.; Zhong, Y.; Zeng, L. Four novel diterpenoids: clavirolides B, C, D, and E from the Chinese soft coral *Clavularia viridis*. *J. Nat. Prod.* **1991**, *54*, 380−385.
(18) Gao, Y.; Du, Y.-Q.; Zang, Y.; Liu, H.-C.; Wan, H.-Y.; Li, J.; Li, X.-W.; Guo, Y.-W. Dolabellane diterpenoids from the Xisha soft coral *Clavularia viridis*. *ACS Omega* **2022**, *7*, 3052−3059.
(19) Wei, X.; Rodríguez, A. D.; Baran, P.; Raptis, R. G. Dolabellane-type diterpenoids with antiprotozoan activity from a southwestern Caribbean gorgonian octocoral of the genus Eunicea. *J. Nat. Prod.* **2010**, *73*, 925−934.
(20) Konno, K.; Fujishima, T.; Liu, Z.; Takayama, H. Determination of absolute configuration of 1,3-diols by the modified Mosher's method using their di-MTPA esters. *Chirality* **2002**, *14*, 72−80.
(21) Lange, G. L.; Lee, M. ^{13}C NMR determination of the configuration of methyl-substituted double bonds in medium- and large-ring terpenoids. *Magn. Reson. Chem.* **1986**, *24*, 656−658.
(22) Chiu, C.; Ling, X.; Wang, S.; Duh, C. Ubiquitin-proteasome modulating dolabellanes and secosteroids from soft coral *Clavularia flava*. *Mar. Drugs* **2020**, *18*, No. e39.
(23) Su, J.; Zhong, Y.; Shi, K.; Cheng, Q.; Snyder, J. K.; Hu, S.; Huang, Y. Clavudiol A and clavirolide A, two marine dolabellane diterpenes from the soft coral *Clavularia viridis*. *J. Org. Chem.* **1991**, *56*, 2337−2344.
(24) Cirne-Santos, C. C.; Teixeira, V. L.; Castello-Branco, L. R.; Frugulhetti, I. C.; Bou-Habib, D. C. Inhibition of HIV-1 replication in human primary cells by a dolabellane diterpene isolated from the marine algae *Dictyota pfaffii*. *Planta Med.* **2006**, *72*, 295−299.
(25) Pardo-Vargas, A.; Ramos, F. A.; Cirne-Santos, C. C.; Stephens, P. R.; Paixão, I. C. P.; Teixeira, V. L.; Castellanos, L. Semi-synthesis of oxygenated dolabellane diterpenes with highly in vitro anti-HIV-1 activity. *Bioorg. Med. Chem. Lett.* **2014**, *24*, 4381−4383.